Atmos. Chem. Phys. Discuss., 15, 6207–6236, 2015
www.atmos-chem-phys-discuss.net/15/6207/2015/
doi:10.5194/acpd-15-6207-2015

Atmospheric Chemistry and Physics
Discussions
Open Access

Laboratory studies of collection efficiency of sub-micrometer aerosol particles by cloud droplets on a single droplet basis

K. Ardon-Dryer, Y.-W. Huang, and D. J. Cziczo

Dept. of Earth, Atmospheric and Planetary Sciences, Massachusetts Institute of Technology, USA

Received: 5 January 2015 – Accepted: 15 February 2015 – Published: 4 March 2015

Correspondence to: K. Ardon-Dryer (karin.ardon@gmail.com) and D. J. Cziczo (djcziczo@mit.edu)

Published by Copernicus Publications on behalf of the European Geosciences Union.

Abstract

An experimental setup has been constructed to measure the Collection Efficiency (CE) of sub-micrometer aerosol particles by cloud droplets. Water droplets of a dilute aqueous ammonium sulfate solution with a radius of ~ 20 µm fall freely into a chamber and collide with sub-micrometer Polystyrene Latex Sphere (PSL) particles of variable size and concentrations. Two RH conditions, ~ 15 and ~ 88 %, hereafter termed "Low" and "High", respectively, were varied with different particles size and concentrations. After passing through the chamber, the droplets and aerosol particles were sent to the Particle Analysis by Laser Mass Spectrometry (PALMS) instrument to determine chemical compositions on a single particle basis. Coagulated droplets had mass spectra that contain signatures from both an aerosol particle and a droplet residual. CE values range from 5.7×10^{-3} to 4.6×10^{-2} for the Low RH and from 6.4×10^{-3} to 2.2×10^{-2} for the High RH cases. CE values were, within experimental uncertainty, independent of the aerosol concentrations. CE values in this work were found to be in agreement with previous experimental and theoretical studies. To our knowledge, this is the first coagulation experiment performed on a single droplet basis.

1 Introduction

The interplay between aerosol particles and water droplets in the atmosphere, especially in clouds, influences both aerosol and cloud properties. The major uncertainty in our understanding of climate arises from the indirect effect of aerosol particles: their ability to affect cloud formation and, consequently, alter the global radiative balance (ICCP, 2007). When an aerosol particle comes in contact with a water droplet the interaction can result in a collision followed by coalescence of the two. This process is known as "collection" or "coagulation". The collection process is considered an important mechanism that can "scavenge", and thereby remove, aerosol particles from the atmosphere (Starr and Mason, 1966; Owe Berg et al., 1970; Hampl and Kerker, 1972;

ACPD
15, 6207–6236, 2015

Pranesha and Kamra, 1996). This process can also influence aerosol and cloud lifetime and thereby affect the global radiation budget (Ladino et al., 2011). In supercooled clouds, where droplets are present at temperatures below 0 °C, the collection process can have an effect on precipitation when the contacting aerosol initiates ice nucleation. The result is the creation of an ice crystal, a process known as "contact nucleation" (Vali, 1996).

Collection efficiency (CE) is the ability of a droplet to coagulate with the aerosol particles within the volume swept out as it falls. Several mechanisms and forces can affect the collection process. These include inertial impaction, Brownian diffusion, interception, electrical and other phoretic forces (see Fig. 1). Inertial impaction is defined as the impaction of particles, those of sufficient inertia that they do not follow their original streamline around the droplet but instead travel close enough to the surface to result in a collision. Brownian motion refers to the movement of the particle due to collisions with air molecules, in this context it results in a "random walk" into the droplet surface.Interception is impaction of particles that follow a streamline that approaches the droplet within a distance of the particle radius. Electrical forces, also commonly termed electro-scavenging or electrophoresis, occur when opposite electrical charges are present on the droplet and the particle resulting in an attraction between the two. Other phoretic forces occur when a droplet evaporates or grows. These phoretic forces include thermophoresis and diffusiophoresis. Thermophoresis takes place when there is a temperature gradient between a droplet and its surroundings. When a droplet evaporates its surface can become colder and aerosols will be drawn inwards. Diffusiophoresis, a counterforce to thermophoresis, occurs when there is a concentration gradient in water vapor, as is the case near an evaporating droplet. Higher water vapor concentration surrounding the droplet "pushes" particles outward. A review of the phoretic forces can be found in Pruppacher and Klett (1997).

The mechanisms described above aredependent on the size of the aerosol particle being collected. Whereas for large particles (radius > 1 µm) inertial effects dominate the collection process, small particle (radius < 0.1µm) motion is dominated by Brownian diffusion. Phoretic and electrical effects have a larger relative impact on particles in an intermediate size range (Wang and Pruppacher, 1977). This intermediate range, ~ 0.1–1 µm, is normally termed the "Greenfield gap", and coincides with an observed minimum in CE (Greenfield, 1957). The particle radius of the Greenfield gap has also been observed to vary with the collecting droplets size (Tinsley et al., 2001).

Many factors, besides particle size, have been observed to affect CE (Byrne and Jennings, 1993). These include particle density (Chate and Kamra, 1997), turbulence (Grover and Pruppacher, 1985) and RH. Lower RH has been observed to correlate with higher CE values, apparently due to phoretic forces (Grover et al., 1977; Tinsley et al., 2001). Droplet size can impact CE, where lower values correlate with larger droplets (Lai et al., 1978; Pranesha and Kamra, 1996). Higher charge also correlates with higher CE, indicative of greater electrical force (Beard, 1974; Wang and Pruppacher, 1977; Lai et al., 1978; Barlow and Latham, 1983; Pranesha and Kamra, 1997a, b; Tinsley et al., 2000). It should be noted that the number of elemental charges used in previous work was often motivated by atmospheric observations: a few tens to hundreds for altostratus and stratocumulus clouds (Phillips and Kinzer, 1958; Beard et al., 2004) and hundreds to thousands in cumulonimbus clouds (Thomson and Iribarne, 1978; Marshall and Winn, 1982).

To date, there have been numerous experimental and theoretical studies of the collection process (Beard, 1974; Grover et al., 1977; Pranesha and Kamra, 1996; Parker et al., 2005; Tinsley et al., 2006). Most of the experimental studies have focused on drizzle and rain drop sizes (Hampl and Kerker, 1972; Deshler, 1985; Pranesha and Kamra, 1997a, b) while few used smaller cloud droplets (Ladino et al., 2011). A list of these studies is provided in Table 1. Note that only a few of the experiments reported aerosol concentrations and none mentioned if different concentrations were compared.

Previous studies have relied on bulk collection of coagulated droplets followed by off-line analysis to assess CE (Hampl et al., 1971; Deshler, 1985; Pranesha and Kamra, 1993; Chate and Kamra, 1997). Off-line analytical instruments include mass spectrometry (Ladino et al., 2011), atomic absorption spectroscopy (Barlow and Latham, 1983;

ACPD
15, 6207–6236, 2015

Pranesha and Kamra, 1996), fluorescence spectrometry (Byrne and Jennings, 1993) and neutron activation analysis (Beard, 1974). The efficiency determined from bulk collection of droplets results in a signal to noise issue where minimal coagulation events can fall below instrumental detection limits. The inability to determine multiple collection events by single droplets is another possible source of error. To our knowledge, no previous study allowed for determination of coagulation on a single droplets basis, which is the relevant condition for many cloud processes, among these contact nucleation. Another limitation of these bulk analytical methods lies in the aerosol type. Since each technique relies on certain property of the aerosol particles (such as fluorescence, radioactivity or atomic absorption), these experiments were restricted to a specific particle type exhibiting that property. These limitations often limit the atmospheric applicability of the results.

The goal of this study was to determine the CE of sub-micrometer aerosol particles by cloud droplets. This study was conducted on a single droplet basis with sensitivity to one or more coagulation events.

2 Experimental methods

2.1 Experimental setup

The CE experiments were performed in the new Massachusetts Institute of Technology Collection Efficiency Chamber (MIT-CEC). A schematic of the system is shown in Fig. 2. Aerosol particles and droplets were generated and separately passed into the MIT-CEC chamber where they could fall and interact in the laminar flow environment of the chamber. Condensed phase water was removed in dryers after the chamber, and the flow containing aerosol particles and droplet residuals was directed to the Particle Analysis by Laser Mass Spectrometry (PALMS) instrument for single particle analysis.

Polystyrene Latex Spheres (PSL) with radius 0.025, 0.125, 0.25 and 0.475 µm were use in the experiments. PSLs were wet generated using a Brechtel Manufacturing, Inc. (BMI, Hayward, CA) Model 9203 Aerosol Generation System. Condensed phase water was removed by in line dryers. Large particle (0.25 and 0.475 µm) concentrations were measured by an Optical Particle Sizer (OPS; TSI, Inc., Shoreview, MN Model 3330). Smaller particles, below the OPS detection threshold, were size selected using a Differential Mobility Analyzer (DMA; BMI, Inc. Model 2002) and their concentrations monitored by a condensation particle counter (CPC; BMI, Inc. MCPC Model 1710). Two aerosol concentrations were used in the experiments: ~ 50 and 100 cm^{-3}. After the particles were generated, but before they enter the chamber, the particle flow either passed directly over a RH sensor (Omega EE08) in a Low RH experiment or through a humidifier and then over the RH sensor in a High RH experiment. The humidifier, a mixing volume containing Milli-Q 18.2 MΩ cm water, was used to increase the RH of the airflow to ~ 88 %. Two additional RH sensors were placed at the chamber top and bottom to monitor the temperature and RH profile. Valves were placed in-line to either block or admit particles depending on the experimental phase described in the following paragraphs.

The overall length of the MIT-CEC is 1.6 m. The chamber was constructed of glass with stainless steel and aluminum ports for connections to the dryers, aerosol and droplet input. The upper part of the chamber, termed the Droplet Generator and Neutralizer (DGN) unit, is a 21 cm long 5 cm diameter stainless steel cylinder. This section contains a commercial droplet generator, a charge neutralizer, and ports for aerosol injection. A mesh grid is used to straighten the particle flow. Droplets are injected vertically downward through a tube so they do not come in contact with the aerosol particles until they reach the lower portion of the DGN. A neutralizer, containing two Polonium-210 strips and 15 cm in length, is placed in the lower part of the DGN. The lower part of the DGN is then connected directly to the main chamber, a single-jacketed glass column with an inner diameter of 5 cm. The length of the jacketed area is 1.4 m. An aluminum cone reducer, 4 cm in length, is attached to the bottom of the main chamber in order to focus the flow into a variable length dryer used for condensed phase water removal prior to analysis with PALMS.

ACPD
15, 6207–6236, 2015

A Microdrop Technologies Dispenser Systems (Microdrop Technologies Norderstedt, Germany Model MD-K-130) was used to generate droplets. This generator, based on piezo-driven inkjet printing technology, generates droplets with ∼ 20 µm radius. A Microdrop CCD camera (Model MD-O-538-85) coupled to imaging optics, yielding a total magnification of 120×, was used to determine droplet size on a daily basis before the generator was set atop the chamber. Droplets were generated at 30 Hz. This is a frequency much lower than used in previous experimental work (e.g., 1000 Hz in Ladino et al., 2011) since detection was accomplished on a single droplet, not bulk, basis. This rate yielded both a coagulation signal with PALMS and minimized possible droplet-droplet collisions.

As mentioned in the previous section, droplet and aerosol charge affect electroscavengin forces and can therefore impact the coagulation rate. To determine the droplets charge, we utilized an electrometer (Liu and Pui, 1974) which was connected to the DG. Using the electrometer, we determined that $\sim 10^4$ elemental charges are imparted to each droplet upon production from the generator. The neutralizer reduces this charge to 400 ± 400 elemental charges.

The droplets were produced from a dilute ammonium sulfate ($(NH_4)_2SO_4$; hereafter AS) solution, 0.08 $g\,L^{-1}$. Dilute AS was used due to its atmospheric relevance as a condensation nucleus and in order to provide a chemically distinct signature for detection of residuals with PALMS. Based on the original droplet size and solution concentration and as verified by PALMS sizing, a single residual particle was ∼ 0.75 µm radius.

The PALMS instrument determines size and chemical composition of an individual aerosol particle. A detailed description of the PALMS instrument has been published previously (Murphy and Thomson, 1995; Cziczo et al., 2006). In brief, particles enter an aerodynamic inlet, which focuses the particle stream. Particles enter a source region where they pass through two 532 nm Nd : YAG laser beams which yields scattering signals that are used to trigger an excimer laser beam (193 nm). The time difference between the two scattering signals provides an aerodynamic size of the particle (Cziczo et al., 2006). The excimer laser ablates and ionizes the particle. The ions from

ACPD
15, 6207–6236, 2015

each detected particle are ejected into a reflectron mass spectrometer and detected at a micro-channel plate (MCP), thus providing a mass spectrum of the particle.

2.2 Data Analysis

Droplet residuals, PSL particles and coagulated droplet each exhibit a distinct size PALMS mass spectrum (Fig. 3). PSL particles had distinct signatures of their carbon chains at mass to charge ratio (M/C) of 12 (C_1), 24 (C_2), 36 (C_3) and 48 (C_4); in many cases the carbons were associated with hydrogen. Droplets residuals had a signature at M/C 18 (NH_4) and 30 (NO). It should be noted that the PSLs did not contain the droplet signature nor did the droplets contain a PSL signature. Coagulated droplets, on the other hand, exhibited mass spectra with signatures from both the droplet residuals and the PSL particles (Fig. 3c). In order to determine the presence or absence of a coagulation event, a Coagulated Index (CI) was developed:

$$\mathrm{CI} = \frac{\text{carbon signal}}{\text{amonium sulfate signal}} \tag{1}$$

Each experiment started by passing only droplets through the chamber. This allowed for a reference case of maximum CI without coagulation based on > 1000 droplets analyzed. After the reference spectra were obtained, aerosol particles were added to the chamber by opening the in-line valves. Each coagulation experiment contained at least 1000 analyzed droplets with a CI value greater than the baseline obtained from the droplet-only phase. CI for each droplet during a typical experiment is plotted in Fig. 4. The leftmost data is the baseline CI, in this case for > 2500 droplets. The coagulation experiment is on the right where 5 coagulation events were observed. Using these data an Experimental Collection Ratio (ECR) was calculated:

$$\mathrm{ECR} = \frac{\text{number of droplets that coagulated}}{\text{total number of droplets}} \tag{2}$$

ACPD
15, 6207–6236, 2015

For this experiment, 5 out of the 1189 droplets experienced coagulation, yielding an ECR of 4.2×10^{-3}.

A CE value, normalized by the number of particles contained within the volume swept out by a falling droplet, was also calculated. This calculation takes into account a droplet's cross section, the aerosol concentration, and the length of the chamber so that comparisons can be drawn between these data and previous experiments using different setups:

$$\mathrm{CE} = \frac{\mathrm{ECR}}{\pi (R_\mathrm{d} + R_\mathrm{a})^2 L A_\mathrm{c}} \tag{3}$$

Where R_d is the droplet radius, R_a is the aerosol radius, L is the length of the chamber and A_c is the aerosol number concentration.

2.3 Theoretical CE models

Previous studies have theoretically determined the CE between droplets and aerosol particles (Slinn and Shen, 1970; Beard, 1974; Wang and Pruppacher, 1977; Grover et al., 1977; Davenport and Peterst, 1978; Wang et al., 1978, 2010; Park et al., 2005; Tinsley et al., 2000, 2006; Chate, 2005; Andronache et al., 2006; Feng, 2007; Croft et al., 2009; Tinsley, 2010; Tinsley and Leddon, 2013). In order to understand our experimental data, we compare them to a theoretical treatment of CE. This treatment includes Brownian diffusion, interception, inertial impaction, thermophoresis, diffusiophoresis and electro-scavenging. The total CE is the sum of these processes. The CE due to Brownian diffusion, interception and inertial impaction are based on Park et al. (2005) which, in turn, expands on Jung and Lee (1998). Thermophoresis, diffusiophoresis and electro-scavenging are based on Wang et al. (2010) which expands

ACPD
15, 6207–6236, 2015

on Davenport and Peterst (1978). The efficiencies used here are:

$$E_{\mathrm{Bdiff}} = 2\left(\frac{\pi\sqrt{3}}{4P_e}\right)^{2/3}\left[\frac{(1-\alpha)\left(3\frac{\mu_\mathrm{w}}{\mu_\mathrm{a}}+4\right)}{\left(1-\frac{6}{5}\alpha^{1/3}+\frac{1}{5}\alpha^2\right)+\frac{\mu_\mathrm{w}}{\mu_\mathrm{a}}\left(1-\frac{9}{5}\alpha^{1/3}+\frac{1}{5}\alpha^2+\alpha\right)}\right]^{1/3} \tag{4}$$

$$E_{\mathrm{int}} = \left[\frac{1-\alpha}{\left(1-\frac{6}{5}\alpha^{1/3}+\frac{1}{5}\alpha^2\right)+\frac{\mu_\mathrm{w}}{\mu_\mathrm{a}}\left(1-\frac{9}{5}\alpha^{1/3}+\frac{1}{5}\alpha^2+\alpha\right)}\right] \tag{5}$$
$$\left[\frac{(D_\mathrm{a}/D_\mathrm{d})}{1+(D_\mathrm{a}/D_\mathrm{d})}+\frac{1}{2}\left(\frac{(D_\mathrm{a}/D_\mathrm{d})}{1+(D_\mathrm{a}/D_\mathrm{d})}\right)^2\left(3\frac{\mu_\mathrm{w}}{\mu_\mathrm{a}}+4\right)\right]$$

$$E_{\mathrm{imp}} = \left(\frac{\mathrm{Stk}}{\mathrm{Stk}+0.35}\right)^2 \tag{6}$$

$$E_{\mathrm{th}} = \frac{4\left[\frac{2Cc\left(K_\mathrm{a}+5\frac{\lambda}{D_\mathrm{d}}K_\mathrm{p}\right)K_\mathrm{a}}{5P\left(1+6\frac{\lambda}{D_\mathrm{d}}\right)\left(2K_\mathrm{a}+K_\mathrm{p}+10\frac{\lambda}{D_\mathrm{d}}K_\mathrm{p}\right)}\right]\left(2+0.6Re^{1/2}Pr^{1/3}\right)(T_\mathrm{a}-T_\mathrm{d})}{D_\mathrm{d}V_\mathrm{d}} \tag{7}$$

$$E_{\mathrm{df}} = \frac{4\left[\frac{T_\mathrm{a}D_w}{P}\left(\frac{M_\mathrm{w}}{M_\mathrm{a}}\right)^{1/2}\right]\left(2+0.6Re^{1/2}Pr^{1/3}\right)\left(\frac{\rho_\mathrm{a}-\rho_\mathrm{d}}{T_\mathrm{a}-T_\mathrm{d}}\right)}{D_\mathrm{d}V_\mathrm{d}} \tag{8}$$

$$E_{\mathrm{ec}} = \frac{16C_c k_{\mathrm{ec}}Q_r q_r}{3\pi\mu_\mathrm{a}D_\mathrm{p}^2 D_\mathrm{a}V_\mathrm{d}} \tag{9}$$

Where, E_{Bdiff}, E_{int}, E_{imp}, E_{th}, E_{df} and E_{es} are Brownian diffusion, interception, inertial impaction, thermophoresis, diffusiophoresis and electro-scavenging efficiencies, respectively. A full definition of all variables is provided in Table 2.

3 Result and discussion

A total of 16 coagulation experiments were performed. The coagulation experiments contained four different aerosol sizes (with radius 0.025, 0.125, 0.25 and 0.475 µm), each at two different concentrations (50 and 100 cm^{-3}) and at two different RH conditions (15 ± 1 % and 88 ± 1 %). A full description of the experiments is summarized in Table 3. All experiments were conducted at room temperature (22.5 ± 1 °C). Droplet radius was 21.6 ± 1 µm. Terminal (settling) velocity was calculated based on the experimental temperature and droplet size. The terminal velocity varied from 4.7 to 5.8 $cm\,s^{-1}$. Average droplet evaporation time was calculated based on the average droplet size and the RH condition: 2.1 and 14.7 s for the Low and High RH cases, respectively.

Each coagulation experiment incorporated between 1039 to 4598 droplets. The droplets that coagulated were identified based on their CI as described in Sect. 2.2. ECRs were based on the ratio between the number of coagulated droplets to the total number of droplets per experiment and these values varied from 6.5×10^{-4} to 8.6×10^{-3} for the Low RH experiments and from 9.6×10^{-4} to 4.9×10^{-3} for the High RH experiments. ECR was higher for the higher aerosol concentration experiments for most particles sizes; this is consistent with higher aerosol concentration increasing the chances for particles to coagulate with droplets.

CE value was calculated for each experiment. CE values, normalized to experimental conditions, ranged from 5.7×10^{-3} to 4.6×10^{-2} for the Low RH experiments and from 6.4×10^{-3} to 2.2×10^{-2} for the High RH experiments (see Fig. 5). These values are in a similar range to that found by previous works (Wang and Pruppacher, 1977; Lai et al., 1978). Shown in Fig. 5, a significant difference in CE values between the two aerosol concentrations (50 and 100 cm^{-3}) was not observed. Most previous experiments did not specify what aerosol concentration were used during their coagulation experiments (Hampl et al., 1971; Lei et al., 1978; Prodi et al., 2014). Those who did specify had a higher aerosol concentration, in most cases above atmospheric relevance outside polluted boundary layers (above 1000 cm^{-3}; Beard, 1974; Wang and

ACPD
15, 6207–6236, 2015

Pruppacher, 1977; Barlow and Latham, 1983; Deshler, 1985; Ladino et al., 2011). The use of these high aerosol concentrations was likely due to the limitation of bulk analysis methods, as discussed in the Introduction, which required a high concentration for adequate signal.

It has been shown theoretically by Wang et al. (1978), Grover and Pruppacher (1985) and Ladino et al. (2011), and experimentally by Grover et al. (1977) that the CE increases with decreasing RH value. This is because a lower RH leads to an increase of the evaporation rate of the droplet, which strengthens the phoretic forces that increases the CE. Two RH conditions were measured in this experimental work, Low (~ 15 %) and High (~ 88 %). The two-point RH trend here is weak, possibly due to relatively fast evaporation. Higher CE values were found for the Low RH experiment at a particle size of 0.025 µm. We suggest that for these small particles Brownian diffusion effects are stronger than phoretic forces.

In the previous experimental studies of coagulation, many considered significantly larger droplets (of drizzle or rain size; Leong et al., 1982; Pranesha and Kamra, 1993; Chate and Kamra, 1997) and particle sizes (super-micrometer; Owe Berg et al., 1970; Hampl and Kerker, 1972). For these reasons, we do not believe a direct comparison to our data is valid. This lack of comparison holds for other studies, using aerosol in a similar size range but with much larger droplets (Hampl et al., 1971; Deshler, 1985; Vohl et al., 2001). The droplets used in the current work were significantly smaller, > 15 times, than those used in the aforementioned experiments. Those studies reported lower CE values than measured here, in some cases by an order of magnitude. It has been shown in previous experimental and theoretical studies that the CE decreases with increasing droplet sizes (Davenport and Peterst, 1978; Wang et al., 1978; Leong et al., 1982; Pranesha and Kamra, 1993). It is likely that some of the differences in CE are also a result of different experimental conditions, such as droplets and/or particle charge.

Two experimental studies, Wang and Pruppacher (1977) and Lai et al. (1978), are comparable to our study and both exhibit CE values in a range similar to our measure-

ACPD
15, 6207–6236, 2015

ments. A comparison is provided in Fig. 6. While difference in CE values appears at some of the measures particles sizes, overall most had a similar range of CE values. It is noteworthy that similar CE values were measured despite different experimental conditions. For example, Wang and Pruppacher (1977) and by Lai et al. (1978) used somewhat larger droplets in their experiments (of 170–340 and 620 µm, respectively). In addition, both works used droplets with higher charges than those used in the current work, 5×10^5–7.1×10^6 elementary charges in Wang and Pruppacher (1977) and 6.6×10^{28}–2×10^{29} elementary charges in Lai et al. (1978). Since it is known that droplets carrying electric charges will have higher CE (Barlow and Latham, 1983; Byrne and Jennings, 1993; Pranesha and Kamra, 1997a, b; Tinsley and Leddon, 2013; Tinsley et al., 2000; Tinsley, 2010) it possible the size and charge conditions offset each other, lending to the comparison to our data. Lai et al. (1978) did not mention the aerosol concentrations or RH conditions used in their work. Wang and Pruppacher (1977) used RH condition similar to that used in this work but with a higher aerosol concentrations.

The most similar conditions to ours are those of Ladino et al. (2011). Ladino et al. used similar droplets (radius of 12.8–20 µm) and particle sizes (radius of 0.05–0.33 µm). Experiments were conducted at RH conditions similar to our High RH experiments (88 ± 2 %). Although most of the experimental conditions were similar, there are noteworthy differences between the CE values of Ladino et al. and those measured in this study, which are lower overall (Fig. 6). The main difference between the two studies is the droplet charge, which has a stronger impact on the electroscavenging force. Ladino et al. used droplets with high charges, $\sim 5 \times 10^4$ elementary charges per droplet (C. Marcolli, personal communication, 2014), which are two orders of magnitude higher than the one used in this study. The higher droplet charge explains the higher CE values compared to those determined in this work.

In order to compare our experimental work with theoretical studies a set of calculations, as described in Sect. 2.3, combining six different forces was conducted. Examples of theoretical forces and CE are given in Fig. 7. The properties used in these calculations included an air temperature of 22.5 °C, a pressure of 981 mb, RH of 50 %, PSL particles with a density of 1000 $kg\,m^{-3}$ of different sizes matching the experiments, a thermal conductivity of 0.1 $kg\,m\,s^{-3}\,K^{-1}$ (Romay et al., 1998), and a droplet radius of 21.6 µm. Droplets were assumed to have 400 elementary charges, the value determined by the electrometer experiments (see Sect. 2.1).

From Fig. 7, the total CE varies for different particle sizes. The contribution of Brownian diffusion decreases rapidly as particle size increases while the contribution of inertial impaction increase rapidly as particle size increases. Interception forces also increase as particle size increases, but its effect is smaller than that of inertial impaction. The contribution of diffusiophoresis is smaller than that of thermophoresis for particles below 0.05 µm. The Greenfield gap is evident in this figure, as the local minimum between the diffusion- and impaction-dominated regimes. This corresponds to a minimum at a particle size of ~ 0.15 µm. From Fig. 7, one can see that electro-scavenging have a significant impact on the curves. Previous work by Wang et al. (1978), Byrne and Jennings (1993) and Tinsley et al. (2000) showed the presence of charge on droplets and aerosol can increases the CE throughout the Greenfield gap.

In order to directly compare theoretical and measured CE, two cases were calculated: (1) droplet radius 21.4 µm and the Low RH value and (2) 21.9 µm and the High RH valu. In both calculations 0, 400 and 800 elementary charges were assumed per droplet; the range of values determined in the electrometer experiments. One elementary charge was used for the particles, consistent with a Boltzmann distribution imparted by the neutralizer. The result of this comparison is shown in Fig. 8, where the points represent the experimental work and the lines represent the theoretical CE. Overall, there is an agreement between the experimental work and the total CE within this droplet charge regime. Differences may be considered a result of conditions not modeled theoretically. Possibilities include rare aerosol doublet and triplet charging and the evaporation rate of the droplets. Regarding the comparison to Ladino et al. (2011), a simulation with a higher elementary charge (5×10^4 per droplet) was also calculated.

This calculation exhibits higher CE values, by an order a magnitude, than the simulated CE lines which appear for our charge conditions (Fig. 8).

4 Conclusions

An experimental setup has been constructed to measure the CE of ~20 µm radius water droplets with sub-micrometer PSL particles of 0.025, 0.125, 0.25 and 0.475 µm radius and concentrations of 50 and 100 cm^{-3}. Two RH conditions, 15 ± 1 % and 88 ± 1 %, were used. Coagulated droplets were identified on a single-droplets basis using a single particle mass spectrometry. CE values ranged from 5.7×10^{-3} to 4.6×10^{-2} for the Low RH and from 6.4×10^{-3} to 2.2×10^{-2} for the High RH cases. CE values were not significantly different from one another in the conditions employed in this work.

The CEs measured here were found to be in agreement with previous experimental studies on droplets and aerosol particles of roughly similar sizes. Differences in measurements appear to be a result of variable (and sometimes undefined) aerosol and droplet charge, which has been theoretically shown to play an important role in CE. This finding highlight the need for explicit determination of droplet and aerosol charge when presenting results of coagulation experiments.

Acknowledgements. We acknowledge the NOAA OAR Climate Program for their support in this project via grant number NA11OAR4310159. We thank Thomas Leisner, Luis Ladino and Sarvesh Garimella for their advice, assistance and guidance. We acknowledge Paul Ziemann and Karl Froyd and Charles Brock for the use of the electrometer and equipment to determine droplet charge. We also thank Claudia Marcolli and Baban Nagare for information about droplet charge in their experiment.

References

Andronache, C., Grönholm, T., Laakso, L., Phillips, V., and Venäläinen, A.: Scavenging of ultrafine particles by rainfall at a boreal site: observations and model estimations, Atmos. Chem. Phys., 6, 4739–4754, doi:10.5194/acp-6-4739-2006, 2006.

Barlow, A. and Latham, K. J.: A laboratory study of the scavenging of sub-micron aerosol by charged raindrops, Q. J. Roy. Meteor. Soc., 109, 763–770, 1983.

Beard, K.: Experimental and numerical collision efficiencies for sub-micrometer particles scavenged by small raindrops, J. Atmos. Sci., 31, 1595–1603, 1974.

Beard, K. V., Ochs, H. T., and Twohy, C. H.: Aircraft measurements of high average charges on cloud drops in layer clouds, Geophys. Res. Lett., 31, L14111, doi:10.1029/2004GL020465, 2004.

Byrne, M. and Jennings, S.: Scavenging of sub-micrometre aerosol particles by water drops, Atmos. Environ., 27, 2099–2105, 1993.

Chate, D.: Study of scavenging of sub-micrometer-sized aerosol particles by thunderstorm rain events, Atmos. Environ., 39, 6608–6619, 2005.

Chate, D. and Kamra, A.: Collection efficiencies of large water drops collecting aerosol particles of various densities, Atmos. Environ., 31, 1631–1635, 1997.

Croft, B., Lohmann, U., Martin, R. V., Stier, P., Wurzler, S., Feichter, J., Posselt, R., and Ferrachat, S.: Aerosol size-dependent below-cloud scavenging by rain and snow in the ECHAM5-HAM, Atmos. Chem. Phys., 9, 4653–4675, doi:10.5194/acp-9-4653-2009, 2009.

Cziczo, D. J., Thomson, D. S. Thompson, T. DeMott, P. J., and Murphy, D. M.: Aerosol mass spectrometry studies of ice nuclei and other low number density particles, Int. J. Mass Spectrom., 258, 21–31, 2006.

Davenport, H. M. and Peters, L. K.: Field studies of atmospheric particulate concentration changes during precipitation, Atmos. Environ., 12, 997–1008, 1978.

Deshler, T.: Measurements of the rate at which sub-micrometer aerosol particles are scavenged by water drops, J. Aerosol Sci., 16, 399–406, 1985.

Feng, J.: A 3-mode parameterization of below-cloud scavenging of aerosols for use in atmospheric dispersion models, Atmos. Environ., 41, 6808–6822, 2007.

Greenfield, S.: Rain scavenging of radioactive particulate matter from the atmosphere, J. Atmos. Sci., 14, 115–125, 1957.

Grover, S. N. and Pruppacher, H. R.: The effect of vertical turbulent fluctuations in the atmosphere on the collection of aerosol particles by cloud drops, J. Atmos. Sci., 42, 2305–2318, 1985.
Grover, S., Pruppacher, H., and Hamielec, A.: A numerical determination of the efficiency with which spherical aerosol particles collide with spherical water drops due to inertial impaction and phoretic and electrical forces, J. Atmos. Sci., 34, 1655–1663, 1977.
Hampl, V. and Kerker, M.: Scavenging of aerosol by a falling water droplet. Effect of particle size, J. Colloid Interf. Sci., 40, 305–308, 1972.
Hampl, V., Kerker, M., Cooke, D. D., and Matijevic, E.: Scavenging of aerosol particles by a falling water droplet, J. Atmos. Sci., 28, 1211–1221, 1971.
IPCC: Climate Change 2007: the Physical Science Basis, contribution of Working Group I to the Fourth Assessment Report of the Intergovernmental Panel on Climate Change, Paris, 2007.
Jung, C. and Lee, K.: Filtration of fine particles by multiple liquid droplet and gas bubble systems, Aerosol Sci. Tech., 29, 389–401, 1998.
Ladino, L.: Experimental study on collection efficiency and contact freezing of aerosols in a new collision chamber, Ph.D. thesis, ETH Zurich, 2011.
Ladino, L., Stetzer, O., Hattendorf, B., Günther, D., Croft, B., and Lohmann, U.: Experimental study of collection efficiencies between sub-micrometer aerosols and cloud droplets, J. Atmos. Sci., 68, 1853–1864, doi:10.1175/JAS-D-11-012.1, 2011.
Lai, K., Dayan, N., and Kerker, M.: Scavenging of aerosol particles by a falling water drop, J. Atmos. Sci., 35, 674–682, 1978.
Leong, K., Beard, K., and Ochs III, H.: Laboratory measurements of particle capture by evaporating cloud drops, J. Atmos. Sci., 39, 1130–1140, 1982.
Liu, B. Y. H. and Pui, D. Y. H.: A sub-micrometer aerosol standard and the primary, absolute calibration of the condensation nuclei counter, J. Colloid Interf. Sci., 47, 155–171, 1974.
Marshall, T. C. and Winn, W. P.: Measurements of charged precipitation in a New Mexico thunderstorm: lower positive charge centers, J. Geophys. Res., 87, 7141–7157, 1982.
Murphy, D. M. and Thomson, D. S.: Laser ionization mass spectroscopy of single aerosol particles, Aerosol Sci. Tech., 22, 237–249, 1995.
Owe Berg, T. G., Gaukler, T. A., and Vaughan, U.: Collisions in washout, J. Atmos. Sci., 27, 435–442, 1970.

Park, S., Jung, C., Jung, K., Lee, B., and Lee, K.: Wet scrubbing of polydisperse aerosols by freely falling droplets, J. Aerosol Sci., 36, 1444–1458, 2005.

Phillips, B. B. and Kinzer, G. D.: Measurement of the size and electrification of droplets in cumuliform clouds, J. Meteorol., 15, 369–374, 1958.

Pranesha, T. S. and Kamra, A. K.: Experimental measurements of collection efficient of micron sized aerosol particles by Targo water drops, J. Aerosol Sci., 24, S415–S416, 1993.

Pranesha, T. S. and Kamra, A. K.: Scavenging of aerosol particles by large water drops. 1. Neutral case, J. Geophys. Res., 101, 23373–23380, 1996.

Pranesha, T. S. and Kamra, A. K.: Scavenging of aerosol particles by large water drops, 2. The effect of electrical forces, J. Geophys. Res., 102, 23937–23946, 1997a.

Pranesha, T. S. and Kamra, A. K.: Scavenging of aerosol particles by large water drops, 3. Washout coefficients, half-lives, and rainfall depths, J. Geophys. Res., 102, 23947–23953, 1997b.

Prodi, F., Santachiara, G., Belosi, F., Vedernikov, A., and Balapanov, D.: Phoretic forces on aerosol particles surrounding an evaporating droplet in microgravity conditions, Atmos. Res., 142, 40–44, 2014.

Pruppacher, H. R. and Klett, J. D.: Microphysics of Clouds and Precipitation, Kluwer, Norwell, 1997.

Romay, F. J., Takagaki, S. S., Pui, D. Y. H., and Liu, B. Y. H.: Thermophoretic deposition of aerosol particles in turbulent pipe flow, J. Aerosol Sci., 2, 943–959, 199.

Slinn, W. and Shen, S.: Anisotropic Brownian diffusion and precipitation scavenging of submicrometer particles, J. Geophys. Res., 75, 2267–2270, 1970.

Starr, J. and Mason, B.: The capture of airborne particles by water drops and simulated snow crystals, Q. J. Roy. Meteor. Soc., 92, 490–499, 1966.

Thomson, B. A. and Iribarne, J. V.: The fate of electrical charges in evaporating cloud droplets, Rev. Geophys. Space Ge., 16, 431–434, 1978.

Tinsley, B. A.: Electric charge modulation of aerosol scavenging in clouds: rate coefficients with Monte Carlo simulation of diffusion, J. Geophys. Res., 115, D23211, doi:10.1029/2010JD014580, 2010.

Tinsley, B. A. and Leddon, D. B.: Charge modulation of scavenging in clouds: extension of Mont Carl simulations and initial parameterization, J. Geophys. Res., 118, 8612–8624, doi:10.1002/jgrd.50618, 2013.

ACPD
15, 6207–6236, 2015

Tinsley, B. A., Rohrbaugh, R. P., Hei, M., and Beard, K. V.: Effects of image charges on the scavenging of aerosol particles by cloud droplets, and on droplet charging and possible ice nucleation processes, J. Atmos. Sci., 57, 2118–2134, 2000.

Tinsley, B., Rohrbaugh, R., and Hei, M.: Electroscavenging in clouds with broad droplet size distributions and weak electrification, Atmos. Res., 59, 115–135, 2001.

Tinsley, B., Zhou, L., and Plemmons, A.: Changes in scavenging of particles by droplets due to weak electrification in clouds, Atmos. Res., 79, 266–295, 2006.

Vali, G.: Ice nucleation – a review, in: Nucleation and Atmospheric Aerosols, edited by: Kulmala, M. and Wagner, P. E., Elsevier, 271–279, 1996.

Vohl, O., Mitra, S., Diehl, K., Huber, G., Wurzler, S., Kratz, K., and Pruppacher, H.: A wind tunnel study of turbulence effects on the scavenging of aerosol particles by water drops, J. Atmos. Sci., 58, 3064–3072, 2001.

Wang, P. and Pruppacher, H.: An experimental determination of the efficiency with which aerosol particles are collected by water drops in subsaturated air, J. Atmos. Sci., 34, 1664–1669, 1977.

Wang, P. K., Grover, S. N., and Pruppacher, H. R.: On the effect of electric charges on the scavenging of aerosol particles by clouds and small raindrops, J. Atmos. Sci., 35, 1735–1743, 1978.

Wang, X., Zhang, L., and Moran, M. D.: Uncertainty assessment of current size-resolved parameterizations for below-cloud particle scavenging by rain, Atmos. Chem. Phys., 10, 5685–5705, doi:10.5194/acp-10-5685-2010, 2010.

ACPD
15, 6207–6236, 2015

Table 1. Experimental results from previous studies of CE.

Reference	Droplets radius (µm)	Aerosol radius (µm)	Aerosol type	Aerosol concentration (cm^{-3})	RH
Starr and Mason (1966)	100–1000	2.25, 2.5, 6.4	Spores, various	Not Given	Not Given
Owe Berg et al. (1970)	1210–1305	7.5–15	PSL	Not Given	Not Given
Hampl et al. (1971)	710–2540	0.2–0.5	AgCl	Not Given	Not Given
Hampl and Kerker (1972)	2540	53–2000	AgCl	Not Given	Not Given
Beard (1974)	200–425	0.35–0.44	$In(C_5H_7O_2)_3$	5×10^4	97–99
Kerker and Hampl (1974)	940–2540	0.15–0.6	AgCl	Not Given	Not Given
Wang and Pruppacher (1977)	150–2500	0.25 ± 0.03	$In(C_5H_7O_2)_3$	10^{17}–10^{18}	23 ± 2
Lai et al. (1978)	620, 820, 980	0.15–0.45	AgCl	Not Given	Not Given
Leong et al. (1982)	56–93	0.58–3.2	MnO_4P_2	Not Given	~ 30
Barlow and Latham (1983)	270–600	0.2–1	Not Given	> 1000	50–70
Deshler (1985)	1200–1300	0.03, 0.06, 0.13	Not Given	2×10^4–1.4×10^5	60–97
Byrne and Jennings (1993)	400–550	0.35–0.88	Not Given	Not Given	50–80
Pranesha and Kamra (1993)	1800, 2100, 2400	0.95, 1.9, 3.2	NaCl	Not Given	Not Given
Pranesha and Kamra (1996)	1800, 2100, 2400	0.95, 1.9, 3.2	NaCl	Not Given	35–50
Pranesha and Kamra (1997a)	1800, 2100, 2400	0.95, 1.9, 3.2	NaCl	Not Given	35–50
Chate and Kamra (1997)	1800, 2100, 2400	1.5, 2, 3	$MgSO_4$ and $MnCl_2$	Not Given	35–50
Vohl et al. (2001)	346, 1680, 2880	0.16–0.24	$In(C_5H_7O_2)_3$	Not Given	40
Ladino et al. (2011) and Ladino (2011)	12.8, 15, 18.2, 20	0.05–0.33	$LiBO_2$	2×10^3	88 ± 2
Prodi et al. (2014)	240–1075	0.2–1	NaCl	Not Given	< 100

ACPD
15, 6207–6236, 2015

Table 2. Definition of acronyms and relevant units.

Parameter	Definitions	units
Cc	Cunningham slip correction factor	[–]
CE	Collection Efficiency	[–]
D_a	Aerosol particles diameter	[m]
D_d	Droplets diameter	[m]
E_{Bdiff}	Brownian diffusion efficiency	[–]
ECR	Experimental collection ratio	[–]
E_{ec}	Electric charges efficiency	[–]
E_{df}	Diffusiophoresis efficiency	[–]
E_{imp}	Inertial impaction efficiency	[–]
E_{int}	Interception efficiency	[–]
E_{th}	Thermophoresis efficiency	[–]
K_a	Thermal conductivity of moist air	[$kg\,m\,s^{-3}\,K^{-1}$]
K_p	Thermal conductivity of particles	[$kg\,m\,s^{-3}\,K^{-1}$]
M_a	Molecular weight of air	[$kg\,mol^{-1}$]
k_{ec}	k constant for E_{ec} calculations equal to 9×10^9	[$Nm^2\,C^{-2}$]
M_w	Molecular weight of water	[$kg\,mol^{-1}$]
P	Atmospheric pressure	[Pa]
Pe	Peclet number	[–]
Pr	Prandtl number of air	[–]
q_r	Mean charge on aerosol particles	[Coulomb, C]
Q_r	Mean charge on droplets	[Coulomb, C]
R_a	Aerosol radius	[m]
R_d	Droplets radius	[m]
Re	Reynolds number	[–]
Stk	Stokes number	[–]
T_a	Temperature of air	[K]
T_d	Temperature at droplets surface	[K]
V_d	Droplets terminal velocity	[$m\,s^{-1}$]
μ_w	Water viscosity	[$kg\,m^{-1}\,s^{-1}$]
μ_a	Air viscosity	[$kg\,m^{-1}\,s^{-1}$]
ρ_a	Water vapor of water at air temperature	[Pa]
ρ_d	Water vapor of water temperature at droplets surface	[Pa]
λ	Mean free path length of air molecules	[m]
$\propto$	Packing density of drops	[m^3]

ACPD
15, 6207–6236, 2015

Laboratory studies of collection efficiency

K. Ardon-Dryer et al.

Table 3. Particle size and concentration, RH, droplets size and total analyzed and Experimental Collection Ratio (ECR; see text for details) for this study.

Experiment	Particle radius (µm)	Particle concentration (cm^{-3})	RH	Droplet radius (µm)	Total number of droplets	EC
1	0.025 ± 0.005	48 ± 3	11 ± 0.1	20.0	1966	2.4×10^{-3}
2	0.025 ± 0.005	96 ± 8	11	20.0	2578	8.6×10^{-3}
3	0.025 ± 0.005	56 ± 1	85 ± 0.9	22.2	3778	1.5×10^{-3}
4	0.025 ± 0.005	100 ± 6	83 ± 0.1	22.2	2446	1.6×10^{-3}
5	0.125 ± 0.01	49 ± 5	13 ± 1.9	22.2	1923	2.0×10^{-3}
6	0.125 ± 0.01	88 ± 20	15 ± 1.4	22.2	2025	4.9×10^{-3}
7	0.125 ± 0.01	50 ± 3	87 ± 0.4	22.2	4598	2.6×10^{-3}
8	0.125 ± 0.01	102 ± 9	88 ± 0.2	22.2	2831	2.5×10^{-3}
9	0.25 ± 0.02	49 ± 2	17 ± 1.2	21.7	1039	6.5×10^{-4}
10	0.25 ± 0.02	92 ± 4	16 ± 1.3	21.7	3282	1.9×10^{-3}
11	0.25 ± 0.02	51 ± 2	94 ± 2.7	22.2	1530	9.6×10^{-4}
12	0.25 ± 0.02	101 ± 18	90 ± 3.4	22.2	1554	3.0×10^{-3}
13	0.475 ± 0.02	52 ± 3	17 ± 0.3	21.7	1050	1.4×10^{-3}
14	0.475 ± 0.02	98 ± 11	20 ± 2.5	21.7	1232	2.9×10^{-3}
15	0.475 ± 0.02	48 ± 10	87 ± 2.3	20.9	1473	1.9×10^{-3}
16	0.475 ± 0.02	99 ± 16	88 ± 0.6	20.9	1049	4.9×10^{-3}

ACPD
15, 6207–6236, 2015

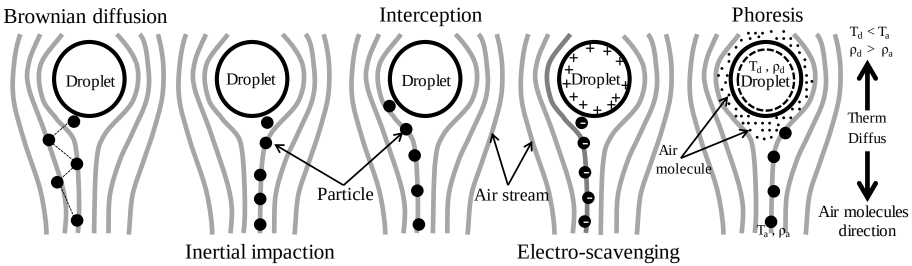

Figure 1. Mechanisms that affect the collection process of aerosol particles by water droplets. The mechanisms, from left to right, are Brownian diffusion, inertial impaction, interception, electro-scavenging and phoresis. T_d and ρ_d are the temperature and water molecule density at the droplet surface while T_a and ρ_a are the ambient temperature and water molecule density. See text for additional description. Figure based on Ladino, 2011.

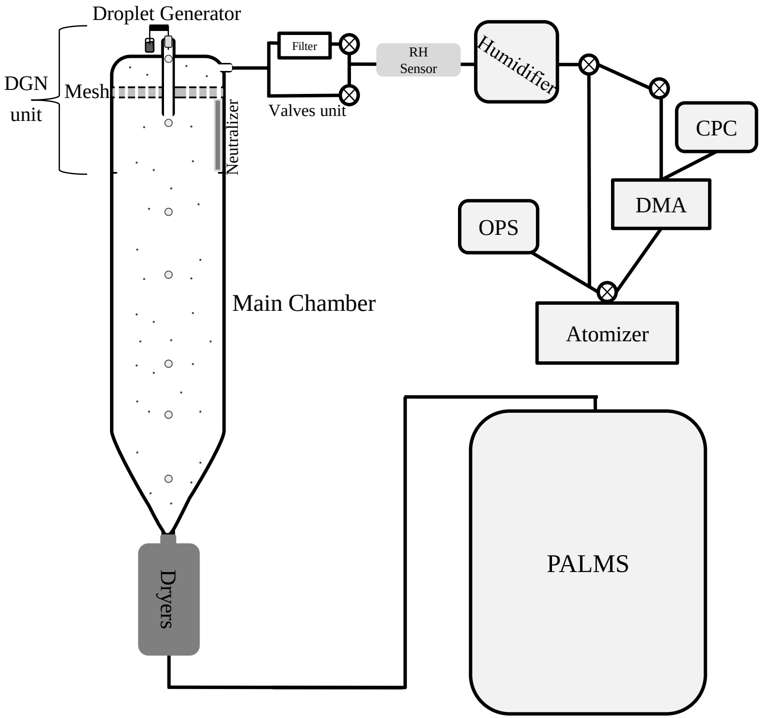

Figure 2. Experimental setup. DGN denotes the Droplet Generation Unit. Additional description is provided in the text.

ACPD
15, 6207–6236, 2015

Laboratory studies of collection efficiency

K. Ardon-Dryer et al.

Title Page
Abstract Introduction
Conclusions References
Tables Figures
◀ ▶
Back Close
Full Screen / Esc
Printer-friendly Version
Interactive Discussion

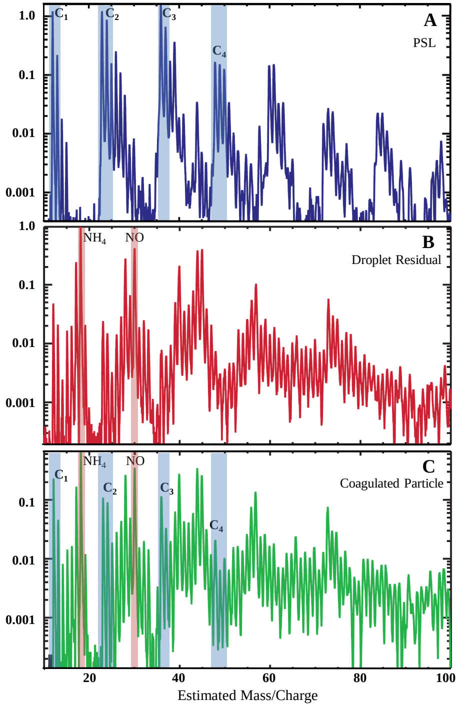

Figure 3. Mass spectrum of a PSL particle **(a)**, an evaporated droplet composed of dilute AS, termed a droplet residual **(b)**, and a coagulated and evaporated droplet that contained both a PSL particle and residual AS **(c)**.

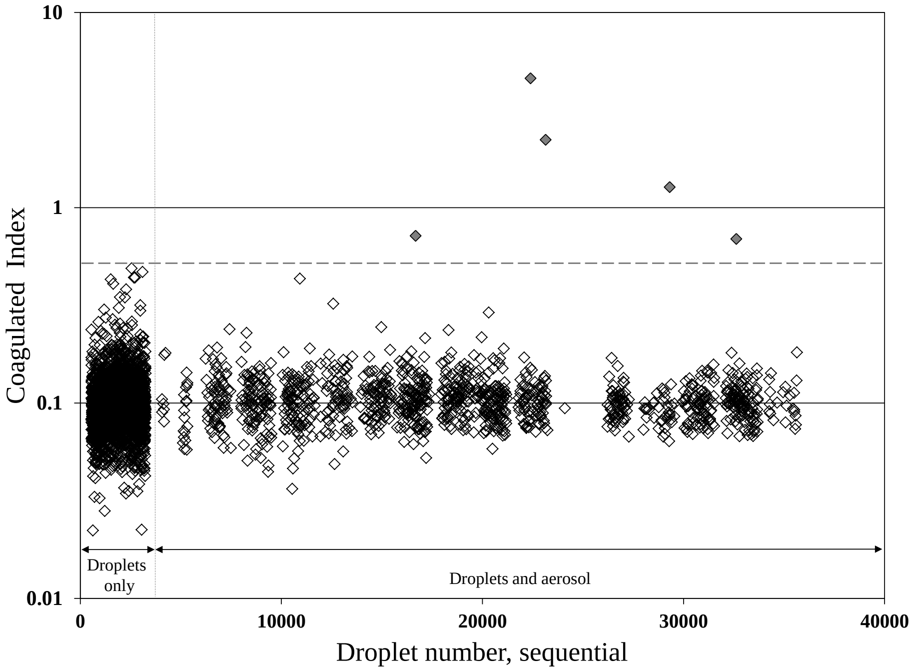

Figure 4. Coagulated Index (CI), the ratio of PSL (aerosol) to AS (droplet residual) signal in a mass spectrum, for a typical experiment. In this experiment the RH was 15 ± 1 %, droplet radius was 20 µm, PSL particles were 0.125 µm radius with a concentration of 100 cm^{-3}. Each data point, the units on the *x* axis, represents the sequential analysis of a single droplet residual over the course of the experiment. Particles which exceed the ratio found when only droplets are analyzed (dashed line; the "Droplets Only" data acquired at the start of each experiment) are considered coagulation events. There are 5 coagulation events during this experimental period.

ACPD
15, 6207–6236, 2015

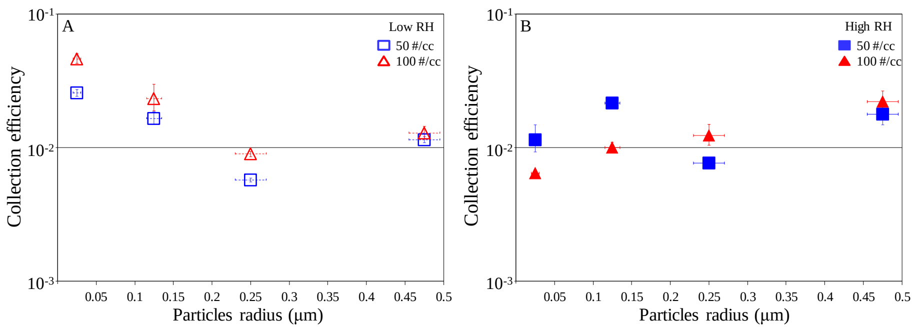

Figure 5. CE as a function of particle radius. Shapes represent different aerosol concentrations. **(a)** Low RH experiments. **(b)** High RH experiments.

ACPD
15, 6207–6236, 2015

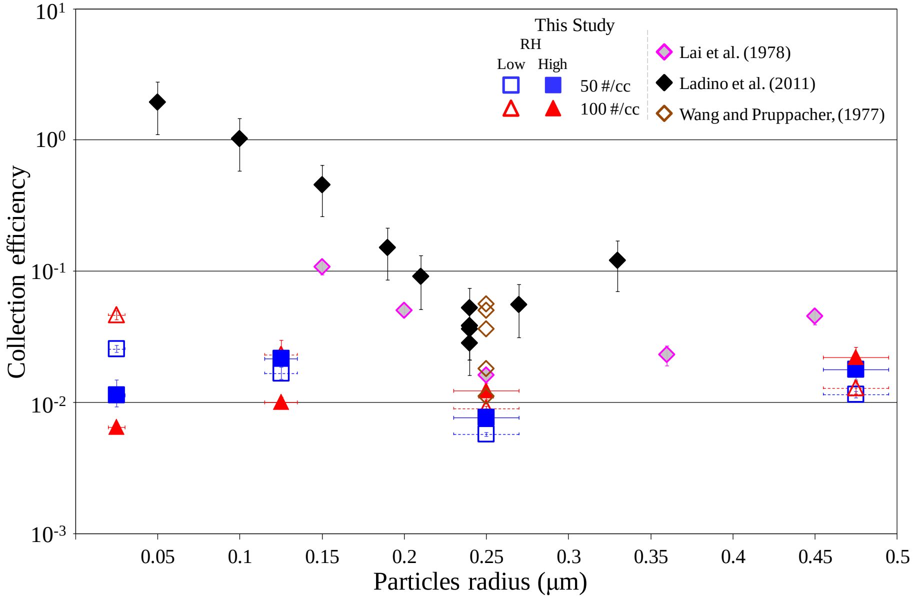

Figure 6. Comparison of CE from this study to previous experimental work. Shapes (square and triangle) represent different aerosol concentrations and the hollow and filled points represent Low and High RH conditions, respectively. Diamond shapes represent previous experimental work. Black diamonds are from Ladino et al. (2011), RH 88 ± 2 % with aerosol concentration 2000 cm^{-3}. Brown diamonds represent are from Wang and Pruppacher (1977), RH of 23 ± 2 % with aerosol concentration ~ 10^{17} cm^{-3}. Pink diamonds are from Lai et at. (1978); there was no information provided regarding the RH or aerosol concentration.

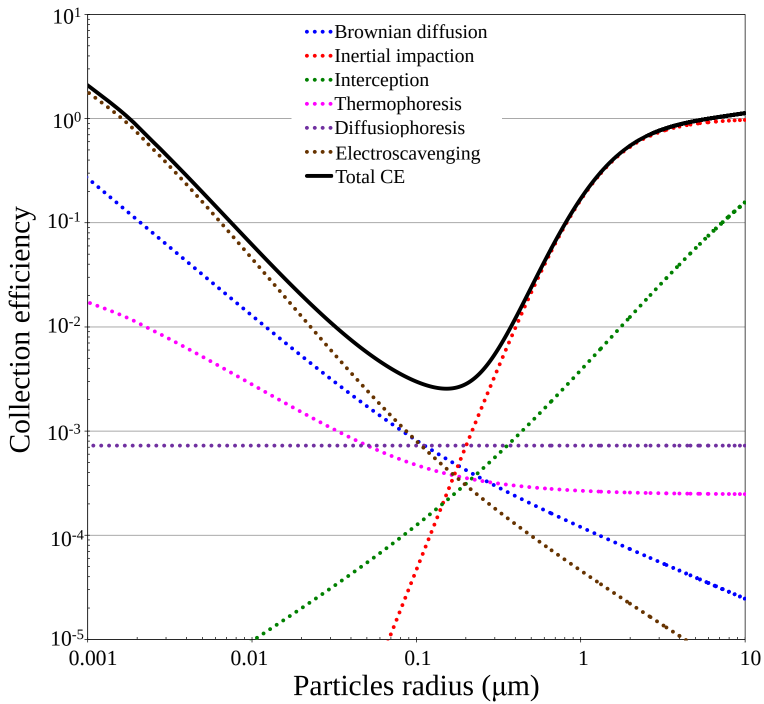

Figure 7. Theoretical CE and the individual contribution of each force. Calculation details are provided in the text. Experimental conditions of 400 elementary charges per droplets and one elementary charge per particle are used for a variable aerosol size, a droplet radius of 21.6 µm, a RH of 50 % and room temperature.

ACPD
15, 6207–6236, 2015

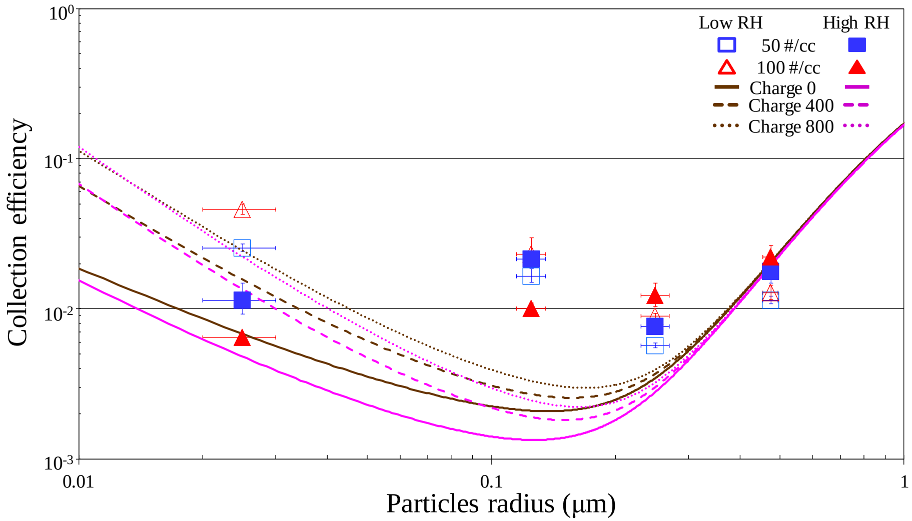

Figure 8. Comparison of CE experimentally determined in this study (points) with theoretical calculations (lines) where the charge number is elemental units per droplet (i.e., the lines span the range of measured droplet charge) and particles are singly charged.